DOI: 10.26599/FSHW.2025.9250840

Contents lists available at SciOpen

Food Science and Human Wellness

journal homepage: https://www.sciopen.com/journal/2097-0765

China Food Publishing Co.

Mechanisms of Phillygenin and Forsythiaside A in Liver Fibrosis Based on Hepatocyte-Derived Exosomes

Sheng-Lin Zhang [1,a], Li-Hong Gong [1,a], Yu-Xin Yao [1], Yan-Zhi Li [1], Yi-Ling Guo [1], Meng-Ling Zhou [1], Chuan-Tao Zhang [1], Xiao-Fang Xie [1], Yao He [1], Cheng Peng [1,*] and Yun-Xia Li [1,*]

[1] *State Key Laboratory of Southwestern Chinese Medicine Resources, Key Laboratory of Standardization for Chinese Herbal Medicine, Ministry of Education, School of Pharmacy, Chengdu University of Traditional Chinese Medicine, Chengdu 611137, China*

ABSTRACT: Liver fibrosis is a dynamic process characterized by excessive extracellular matrix (ECM) deposition due to chronic liver injury. Emerging evidence highlights the pivotal role of intercellular crosstalk in hepatic fibrogenesis, particularly via exosomes mediated communication. *Forsythia suspensa* (Thunb.) Vahl, a traditional Chinese herb with culinary uses such as in teas, congee, and soups, has garnered attention for its medicinal properties. Notably, its bioactive constituents, phillygenin (PHI) and forsythiaside A (FA), exhibit significant antifibrotic potential. This study aimed to investigate the therapeutic mechanisms of PHI and FA in liver fibrosis, focusing on their modulation of LO2 cell-derived exosomes and their subsequent effects on hepatic stellate cell (HSC) activation and macrophage polarization. Initially, we explored the efficacy of PHI and FA on liver fibrosis using a mouse model. We then validated the effects of PHI and FA in an LO2 cell injury model and explored the underlying mechanisms. To further elucidate intercellular interactions, we isolated LO2 cells-derived exosomes and assessed their impact on LX2 and THP-1 cells in co-culture systems. Our results revealed that PHI and FA alleviated liver fibrosis by inhibiting hepatocytes apoptosis, oxidative stress, and inflammatory responses. Furthermore, PHI and FA regulate LO2 cell-derived exosomes to suppress HSC activation and macrophage M1 polarization. In summary, this study elucidates how PHI and FA modulate hepatocyte-HSC-macrophage crosstalk, providing mechanistic insights into their antifibrotic actions. These findings contribute to the understanding of liver fibrosis pathogenesis and offer theoretical support for the development of novel antifibrotic therapies based on traditional Chinese medicine.

Keywords: Liver fibrosis; Phillygenin; Forsythiaside A; LO2 cell-derived exosomes

1. Introduction

Liver fibrosis is defined as a pathological imbalance between tissue injury and repair, characterized by excessive accumulation of fibrous connective tissue. This process is typically driven by activation of hepatic stellate cells (HSCs) and subsequent overproduction of extracellular matrix (ECM)[1]. Liver fibrosis progression is mediated by diverse etiological factors, notably viral hepatitis (e.g., HBV and HCV), chronic alcohol consumption, non-alcoholic fatty liver disease (NAFLD), metabolic disorders, and liver injury from drugs[2-5]. Although liver fibrosis is a reversible pathological condition[6], a lack of timely diagnosis and

[a]Sheng-Lin Zhang and Li-Hong Gong contributed equally to this work.
***Corresponding author**
cdtcmpengcheng@126.com; lyxtgyxcdutcm@163.com

Received 29 March 2025
Received in revised from 14 June 2025
Accepted 31 July 2025

treatment can lead to its progression into irreversible liver cirrhosis or potentially hepatocellular carcinoma[2]. Currently, effective strategies to reverse established fibrosis are unavailable, highlighting the critical demand for developing safe and effective antifibrotic agents.

The treatment of liver fibrosis benefits from the unique advantages of traditional medicine. Forsythiae Fructus, the dried fruit of *Forsythia suspensa* (Thunb.) Vahl, is a widely used traditional Chinese medicine renowned for its heat-clearing, detoxifying, swelling-reducing, and wind-heat dispersing effects. When utilized as a functional food in culinary applications such as teas, congees, and soups, Forsythiae Fructus maintains its heat-clearing and detoxifying properties properties. Emerging pharmacological evidence has demonstrated that Forsythiae Fructus possesses notable anti-inflammatory, antioxidant, and antiviral properties[7, 8]. Phillygenin (PHI) and forsythiaside A (FA) are the primary active components extracted from Forsythiae Fructus and have emerged as particularly promising antifibrotic agents against liver fibrosis[9-12]. Mechanistic studies reveal that PHI exerts its antifibrotic effects through modulation of gut microbiota and bile acid metabolism[11, 13]. Besides, FA ameliorated liver fibrosis by regulating bile acids homeostasis and inhibiting HSCs activation[9, 12]. However, current studies on the mechanisms of Forsythiae Fructus mainly focus on individual chemical components and specific pathways, with limited consideration of the complex, dynamic interplay of pathophysiological mechanisms during disease progression.

Studies have been increasingly showing that the progression of fibrosis is mediated through complex intercellular crosstalk among diverse hepatic cell populations[14-16]. As critical mediators of cell-to-cell communication,, exosomes play pivotal roles in modulating both physiological and pathological processes across multiple biological systems[17]. Exosomes are a class of extracellular vesicles (EVs) with diameters ranging from 30 to 150 nm, and carry a sophisticated molecular cargo comprising proteins, lipids, and RNAs[18]. Studies have shown that exosomal miR-222 derived from Hepatitis B virus (HBV)-infected LO2 cells promotes LX2 cell activation through suppression of TFRC-induced ferroptosis, thereby accelerating liver fibrogenesis[19]. Furthermore, exosomes derived from mesenchymal stem cells (MSCs) have been shown to modulate macrophage phenotypes, thereby improving the hepatic inflammatory microenvironment, promoting tissue repair, and consequently alleviating liver fibrosis[15]. These findings highlight the pivotal, role of exosome-mediated intercellular communication in liver fibrosis pathogenesis and treatment, establishing it as a promising therapeutic target in this field.

The hepatic homeostatic balance is maintained through complex cellular crosstalk among diverse liver cell populations, including hepatocytes, HSCs, and liver macrophages[14, 20]. As the principal functional units of the liver, hepatocytes play a central role in orchestrating metabolic processes and maintaining organ function. When exposed to pathogenic stimuli and damaged, hepatocytes undergo progressive cellular damage characterized by degenerative changes and eventual necrosis. This pathological progression leads to the release of damage-associated molecular patterns (DAMPs), reactive oxygen species (ROS), and other mediators[21]. These signaling molecules trigger macrophage activation, leading to the secretion of pro-fibrogenic mediators such as transforming growth factor-beta 1 (TGF-β1), tumor necrosis factor-alpha

(TNF-α), and platelet-derived growth factor (PDGF). These cytokines subsequently initiate a cascade of molecular events that drive HSCs activation and their differentiation into myofibroblasts[14]. The activated myofibroblasts then engage in excessive ECM synthesis and deposition, ultimately culminating in progressive liver fibrosis[14]. Therefore, strategies aimed at reducing hepatocyte injury through anti-inflammatory and antioxidative mechanisms, inhibiting macrophage polarization, and suppressing HSC activation are critical for preventing liver fibrosis[22-25]. Emerging evidence suggests that timely intervention in the fibrogenic cascade, particularly through restoration of hepatocyte function, precise modulation of macrophage polarization, and inhibition of HSC activation, may effectively attenuate or reverse fibrotic processes in the liver[12, 24, 26]. However, the precise molecular mechanisms by which Forsythiae Fructus exerts its anti-fibrotic effects remain to be fully elucidated, particularly its impact on exosome-mediated intercellular communication and the downstream signaling pathways involved in this process.

Therefore, this study was designed to investigate the therapeutic potential of PHI and FA in a murine model of CCl_4-induced liver fibrosis and to explore their modulatory effects on HSCs activation and macrophage polarization mediated through hepatocyte-derived exosomes. Our research aims to further elucidate the anti-fibrotic mechanisms of PHI and FA, while simultaneously providing mechanistic insights into hepatic fibrogenesis and facilitating the development of novel therapeutic strategies for clinical application.

2. Materials and methods

2.1. Materials

PHI (Cat. No. 487-39-8), FA (Cat. No. 79916-77-4) and colchicine (Cat. No. 64-86-8) were purchased from MUST Bio-Technology Co., Ltd. (Chengdu, China). Olive oil (Cat. No. 8001-25-0) and sodium carboxymethyl cellulose (CMC-Na) (Cat. No. 9004-32-4) were collected from Chron Chemicals Co., Ltd. (Chengdu, China). Animal total RNA isolation kit (Cat. No. R210801) and Genious 2X SYBR Green Fast Quantitative Real-time PCR (qPCR) Mix (Cat. No. 210401) were obtained from Foregene Co., Ltd. (Chengdu, China). Carbon tetrachloride (CCl_4, Cat. No. 56-23-5) was purchased from Adamas-Beta Co., Ltd. (Shanghai, China). Lipopolysaccharide (LPS, from E.Coli 055: B5) was purchased from Sigma (Sigma-Aldrich, China). Dulbecco's modified Eagle's medium (DMEM, Cat. No. C11995500BT) was purchased from Gibco (USA). Fetal bovine serum (FBS, Cat. No. 164210-50) was purchased from Procell (Wuhan, China). 0.25% trypsin solution (containing EDTA, Cat. No. G4002), anti-fluorescence quenching mounting medium (Cat. No. G1401) and BCA protein assay kit (Cat. No. G2026) were purchased from Servicebio (Wuhan, China). ALT biochemical kit (Cat. No. C009-2-1), AST (Cat. No. C010-2-1) biochemical kit and HYP biochemical kit (Cat. No. A030-2-1) were purchased from Nanjing Jiancheng Bioengineering Institute (Nanjing, China). T-SOD assay kit (Cat. No. E-BC-K020-M) and MDA assay kit (Cat. No. E-BC-K025-M) were purchased from Elabscience Biotechnology Co., Ltd (Wuhan, China). GSH assay kit (Cat. No. G20210524C) was purchased from Nanjing Jiancheng Bioengineering Institute (Nanjing, China). HA assay kit (Cat. No. MM-0514M1), LN assay kit (Cat. No. MM-0161M1), PC-III assay kit (Cat. No.

MM-44669M1) and Col-IV assay kit (Cat. No. MM-0297M1) were purchased from Elabscience Biotechnology Co., Ltd (Wuhan, China). TGF-β1 assay kit (Cat. No. E-EL-0162c), IL-1β assay kit (Cat. No. E-EL-M0037c) and TNF-α assay kit (Cat. No. E-EL-M3063) were purchased from Nanjing Jiancheng Bioengineering Institute (Nanjing, China).

2.2. In vivo experimental methods

2.2.1. Animals and treatments

A total of 138 male ICR mice (20 ± 2 g body weight) were obtained from Chengdu Dashuo Experimental Animals Co., Ltd. (Chengdu, China). The animals were housed under controlled environmental conditions (temperature: (23 ± 2) ℃; humidity: 50% ± 20%) with ad libitum access to food and water. Following a 7-day acclimatization period, the animals were allocated into 3 experimental groups: normal control (n=18), vehicle control (n=18), and CCl_4-induced model group (n=102). During the subsequent 14-day period, 3 mice from each group were sacrificed for serum and hepatic tissue collection. The remaining CCl_4 model animals were subsequently randomized into 8 treatment groups: CCl_4 model, colchicine (0.1 mg/kg), PHI (7.5, 15, and 30 mg/kg), and FA (15, 30, and 60 mg/kg) treatment groups. PHI was prepared in 0.5% CMC-Na solution, while colchicine and FA was dissolved in normal saline. The specific model establishment methods and drug treatment methods are shown in Table 1.

Tabel 1 Modeling Methods and Drug Treatment in this Study

Group	Intraperitoneal injection (Three times a week in 1-5 weeks)	Intragastric administration (Once a day in 3-5 weeks)
Normal control group	N/A	Normal saline (10 mL/kg)
Vehicle control group	Olive oil (2 mL/kg)	0.5% CMC-Na (10 mL/kg)
CCl_4 group	10% CCl_4 (2 mL/kg)	Normal saline (10 mL/kg)
CCl_4 + 0.1 mg/kg colchicine	10% CCl_4 (2 mL/kg)	0.1 mg/kg colchicine (dissolved in normal saline)
CCl_4 + 7.5 mg/kg PHI	10% CCl_4 (2 mL/kg)	7.5 mg/kg PHI (dissolved in CMC-Na)
CCl_4 + 15 mg/kg PHI	10% CCl_4 (2 mL/kg)	15 mg/kg PHI (dissolved in CMC-Na)
CCl_4 + 30 mg/kg PHI	10% CCl_4 (2 mL/kg)	30 mg/kg PHI (dissolved in CMC-Na)
CCl_4 + 15 mg/kg FA	10% CCl_4 (2 mL/kg)	15 mg/kg FA (dissolved in normal saline)
CCl_4 + 30 mg/kg FA	10% CCl_4 (2 mL/kg)	30 mg/kg FA (dissolved in normal saline)
CCl_4 + 60 mg/kg FA	10% CCl_4 (2 mL/kg)	60 mg/kg FA (dissolved in normal saline)

Throughout the experiment, three mice per group were euthanized weekly. Upon study completion, all remaining animals were euthanized, with serum and hepatic tissues collected for subsequent analysis. Tissue samples were either fixed in 4% paraformaldehyde or preserved at -80℃ in an ultra-low temperature freezer for further investigation.

This research protocol received ethical clearance from the Animal Experiment Ethics Committee of Chengdu University of Traditional Chinse Medicine (ethical approval number: 2024084). All experimental procedures strictly adhered to the ethical guidelines established in the “Guide for the Care and Use of Laboratory Animals”, ensuring proper animal welfare standards were maintained throughout the study.

2.2.2. Histopathological analysis

Hepatic specimens were preserved in 4% paraformaldehyde solution for 24 h, followed by sequential ethanol dehydration and paraffin embedding. Tissue sections of 4 μm thickness were prepared for histological analyses via hematoxylin-eosin (HE) staining protocol. Morphological analysis and digital imaging were conducted using an upright microscope (Eclipse Ci-L, Nikon, Japan).

Subsequent sections were processed for Masson's trichrome staining following the same protocol. Collagen deposition was quantified using ImageJ software by calculating the percentage of collagen-positive pixels per visual field.

2.2.3. Measurement of liver function indicators

Hepatic tissue samples were precisely weighed and homogenized in ice-cold buffer at a 1:9 (w/v) tissue-to-buffer ratio. After centrifugation at 2500 × g (10 min, 4℃), supernatants were collected for biochemical analysis. Hepatic function markers (ALT, AST) and collagen deposition marker (HYP) were quantified using commercial assay kits according to manufacturer protocols.

2.2.4. Measurement of oxidative stress indicators

Hepatic tissue samples were precisely weighed and homogenized in ice-cold buffer at a 1:9 (w/v) tissue-to-buffer ratio. After centrifugation at 2500 × g (10 min, 4℃), supernatants were collected for oxidative stress analysis. Total superoxide dismutase (T-SOD), malondialdehyde (MDA), and glutathione (GSH) levels were quantified using commercial assay kits per manufacturer protocols.

2.2.5. Elisa analysis

The hepatic levels of key fibrotic and inflammatory markers, including hyaluronic acid (HA), laminin (LN), type III procollagen (PC-III), type IV collagen (Col-IV), transforming growth factor-β1 (TGF-β1), interleukin-1β (IL-1β), and tumor necrosis factor-α (TNF-α), were quantified using enzyme-linked immunosorbent assay (ELISA) kits following the manufacturer's recommended protocols.

2.2.6. Immunohistochemistry analysis

Paraffin-embedded hepatic sections underwent immunohistochemical processing. Following deparaffinization and rehydration, antigen retrieval was performed using citric acid buffer (pH 6.0) in a microwave oven. Endogenous peroxidase activity was blocked with 3% hydrogen peroxide treatment (25 min, room temperature, dark conditions). After three 5-minute PBS (pH 7.4) washes, non-specific binding sites were blocked with 3% bovine serum albumin (30 min, room temperature). Sections were incubated overnight at 4℃ with primary antibodies against α-SMA (1:1000, GB111364, Servicebio) and collagen I (1:1000, GB11022-3, Servicebio). Following three 8-minute PBS washes, sections were incubated with fluorescent-conjugated secondary antibodies (1:200, GB23303, Servicebio) for 2 h at room temperature. The immunoreactivity was visualized using DAB chromogen, followed by nuclear counterstaining, dehydration, and mounting. Protein expression patterns were analyzed using laser scanning confocal microscopy.

2.3. In vitro experimental methods

2.3.1. MTT assay

LO2 cells at 80% confluence were harvested and seeded into sterile 96-well plates at a density of 5×10^3 cells per well. After 24 h of incubation at 37℃ in a CO_2 incubator, different concentrations of PHI (0, 5, 10, 20, 40, 80, 100, 200 μg/mL) or FA (0, 6.25, 12.5, 25, 50, 100, 150, 300 μg/mL) dissolved in DMEM containing 1% FBS were added, with 6 replicates per group and a control group. Following 24 h treatment, 20 μL MTT solution was added per well and incubated (4 h, 37℃, dark). The solution was then removed, and 150 μL of DMSO was added. After thorough mixing, absorbance was measured at 490 nm using a microplate reader.

2.3.2. Cell culture and treatment

LO2 cells were maintained in DMEM with 10% FBS and 1% antibiotics, while LX2 and THP-1 cells were cultured in RPMI-1640 with the same supplements. LO2 cells (1×10^6 cells/well) were plated in six-well plates and divided into eight groups: (1) control; (2) model (100 ng/mL LPS + 5 mmol/L ATP); (3) PHI-L (10 μg/mL PHI); (4) PHI-M (20 μg/mL PHI); (5) PHI-H (40 μg/mL PHI); (6) FA-L (37.5 μg/mL FA); (7) FA-M (75 μg/mL FA); (8) FA-H (150 μg/mL FA). All groups except the control received LPS and ATP.

2.3.3. Real-Time Quantitative PCR (RT-qPCR) analysis

Total RNA from cells was extracted using the Animal Total RNA Isolation Kit, while exosomal RNA was isolated using the Viral RNA Isolation Kit following the manufacturer's protocol. RNA purity was assessed via OD260/280 measurements on a Nucleic Acid/Protein Analyzer. cDNA was synthesized with 5X ABScript III RT Mix for mRNA and 2 × RT Easy™ Mix for miRNA. RT-qPCR was performed using Genious 2X SYBR Green Fast qPCR Mix on a CFX96 Real-Time PCR System (Bio-rad) under the following conditions: 95℃ for 3 min, followed by 40 cycles of 95℃ for 5 s and 60℃ for 30 s. GAPDH and U6 were used as endogenous controls for mRNA and miRNA, respectively. Data were analyzed with the $2^{-\Delta\Delta Ct}$ method. All qPCR primers (synthesized by Tsingke Biotechnology Co., Ltd.) are listed in Table 2.

Table 2 Primer sequences for RT-qPCR.

Gene	Forward primer (5′-3′)	Reverse primer (5′-3′)
Bax	CCCGAGAGGTCTTTTTCCGAG	CCAGCCCATGATGGTTCTGAT
Bcl2	TCACTTGTGGCCCAGATAGG	GATAACGGAGGCTGGGATGC
Caspase3	CATGGAAGCGAATCAATGGACT	CTGTACCAGACCGAGATGTCA
TLR4	GGGTATTTGACACCCTCCATAG	CAAGAGTGCTGAGGGAATACAG
P2X7	GACGCTCTGTTCCTCTGACC	TCCGGTCTGAATTCCTTTGCT
NLRP3	TTCGGAGATTGTGGTTGGGG	CTTCTGGTTGCTGCTGAGGA
NOX4	CCAGATGTTGGGGGATTGTGT	GAGTGTTCGGCACATGGGTA
Nrf2	CTTCTAGTTCGGACGCGGTG	ATCAAATCCATGTCCTGTCCCT
HO-1	TGTTGGAGCCACTCTGTTCC	GCTCAAAAACCACCCCAACC
CD71	TCGTGAGGCTGGATCTCAAAA	CCTTACTATACGCCACATAACCC
CD36	GGCTGTGACCGGAACTGTG	AGGTCTCCAACTGGCATTAGAA
α-SMA	GTTACGAGTTGCCTGATGG	AGGTGGTTTCATGGATGC
GAPDH	GGAGTCCACTGGCGTCTTCA	GTCATGAGTCCTTCCACGATACC

2.3.4. Western blotting

Cells were washed 3 times with PBS and then lysed on ice with 150 μL of RIPA buffer (RIPA buffer: PMSF: protein phosphatase inhibitor = 100:1:1). After 5-min incubation, lysates were sonicated (3 min, ice

bath) and centrifuged (12,000 × g, 15 min, 4℃) to collect protein supernatants. Additionally, cytoplasmic and nuclear proteins were extracted from LO2 cells using the Nuclear Protein Extraction Kit, following the manufacturer's protocol. Protein concentrations were quantified by BCA assay and normalized with lysis buffer. Protein loading buffer (4:1 ratio with total protein) was added, and the mixture was heated at 100℃ for 10 min. Equal protein amounts were loaded onto a 10% SDS-PAGE gel for electrophoresis, then transferred to PVDF membranes. After blocking with 5% BSA for 1 h at room temperature, the membrane was incubated overnight at 4℃ with primary antibodies against Bax, Bcl-2, Nrf2, HO-1, P2X7, NLRP3, TLR4, NOX4, and GAPDH. Following three washes, the membrane was incubated with secondary antibodies (1:5000 dilution) for 1 h at room temperature. Signals were detected using an ECL kit and imaged with a gel imager. The optical density was quantified using ImageJ software.

2.3.5. Isolation and purification of LO2 cell-derived exosomes

2.3.5.1. Preparation of exosome-free serum

Place heat-inactivated FBS into ultracentrifuge tubes and balance the weight using an electronic balance. Carefully load tubes into a fixed-angle rotor, then centrifuge at 170,000 × g (4℃) for 6 h. Following centrifugation, the supernatant was aseptically collected and subjected to filtration using a 0.22 μm membrane filter to ensure bacterial removal. The processed serum was then aliquoted into pre-sterilized microcentrifuge tubes and preserved at -80℃ for subsequent experimental applications.

2.3.5.2. Collection of culture supernatant

LO2 cells were seeded into 175 cm² culture flasks and incubated until reaching 70%–80% confluency. After aspirating the medium and washing cells thrice with PBS, experimental groups (control, model, PHI-treated, and FA-treated) were established by replacing the medium with exosome-depleted medium containing 1% FBS and respective treatments. Following 48-hour incubation, conditioned medium from each group was collected for exosome isolation.

2.3.5.3. Isolation and purification of exosomes

In this study, exosomes were isolated from LO2 cells through differential ultracentrifugation, utilizing sequential low-speed and high-speed centrifugation to obtain exosomes of uniform size. The specific steps are shown in Table 3.

Table 3 Steps of differential ultracentrifugation.

Step	Procedure Name	Operation Method
1	Cell removal	Centrifuge at 300×g, 4℃, for 10 min; collect the supernatant.
2	Removal of dead cells	Centrifuge at 2000×g, 4℃, for 10 min; collect the supernatant.
3	Removal of cell debris	Centrifuge at 10,000×g, 4℃, for 30 min; collect the supernatant and filter through a 0.22 μm membrane.
4	Concentration	Use a 100 kD ultrafiltration tube to concentrate the supernatant to approximately 35 mL.
5	Ultracentrifugation	Centrifuge at 100,000×g, 4℃, for 70 min; carefully discard the supernatant.
6	Purification	Resuspend the exosome pellet in PBS, centrifuge at 100,000×g, 4℃, for 70 min; carefully discard the supernatant.
7	Exosome collection	Resuspend exosomes obtained from every 200 mL of cell culture supernatant in

100-200 μL PBS, aliquot, and store at -80℃ for long-term preservation.

2.3.6. Characterization of LO2 cell-derived exosomes

Exosomes were characterized by: (1) transmission electron microscopy (TEM) for morphological analysis; (2) nanoparticle tracking analysis (NTA) for size distribution; and (3) Western blot detection of exosomal markers (CD63, TSG101, Alix).

2.3.7. Cell Co-Culture Treatment

THP-1 cells were differentiated into macrophages via 48-h stimulation with 100 ng/mL PMA. LX2 cells were trypsinized at 90% confluence, reseeded into new dishes 24 h prior to treatment, and incubated. After confirming THP-1 differentiation or attaining 80% LX2 confluence, medium was aspirated. Exosomes (C-Exo, M-Exo, PHI-Exo, FA-Exo) isolated from LO2 cells were adjusted to a final concentration of 10 μg/mL using fresh medium supplemented with 1% FBS. These diluted exosome solutions were then added to the THP-1 or LX2 cells for co-culture over 24 h.

2.3.8. Immunofluorescence staining

PKH67-labeled exosomes were prepared by incubating 10 μg LO2-derived exosomes with freshly mixed PKH67 dye (1:9 in Diluent C) at 4℃ for 15 min (light-protected). Unbound dye was removed via ultracentrifugation (120,000 × g, 90 min, 4℃). For co-culture, confocal dishes were pre-coated with 1 mL of culture medium (37℃, 15 min). When LX2 cells achieved 90% confluency, they were trypsinized and diluted in RPMI 1640 complete medium to a final density of 5×10^5 cells/mL. In a parallel procedure, THP-1 cells were adjusted to a concentration of 1×10^6 cells/mL. The medium in the confocal dishes was aspirated, and 200 μL of the cell suspension was introduced into the bottom wells. After a 2-hour incubation to facilitate cell adhesion, complete medium was gently supplemented to reach a total volume of 1 mL. At 80% confluency, cells received 1% FBS-medium containing 10 μg/mL exosomes and were co-cultured for 4 h.

Cells were washed thrice with PBS, fixed in 4% paraformaldehyde (15 min), permeabilized with 0.1% Triton X-100 (10 min), and blocked with 5% BSA (30 min, room temperature). Next, the cells were exposed to primary antibodies targeting Caveolin or Clathrin and incubated at 4℃ overnight. After three PBS washes, secondary antibody incubation proceeded (1 h, RT, light-protected). Subsequently, the cells were washed 3 more times, and nuclei were stained with DAPI in the dark for 10 min. Following 3 washes, 100 μL anti-fluorescence quenching mounting medium was applied to each dish, and the samples were stored at 4℃ in the dark. Imaging was performed using a laser confocal microscope.

2.4. Statistical analysis

Statistical analyses were performed using SPSS version 26.0. Quantitative data are expressed as mean ± standard deviation (SD). Graphical representations were generated using GraphPad Prism software. Intergroup comparisons were conducted using either one-way ANOVA or non-parametric tests, as appropriate. A probability value of less than 0.05 ($P < 0.05$) was considered statistically significant.

3. Results

3.1. PHI and FA Inhibit CCl_4-induced liver fibrosis in mice

3.1.1. PHI and FA alleviate CCl_4-induced hepatic pathological and functional changes

HE staining results (Weeks 1-4) appear in Supplementary Fig. 1, while week 5 data are shown in Fig. 1A. Distinct histological differences emerged between groups. In the normal and vehicle control groups, the liver displayed clear lobular structures with tightly arranged hepatocytes, which exhibited loose or vacuolated cytoplasm. Conversely, CCl_4 model mice displayed pronounced steatosis (cytoplasmic lipid vacuoles), hepatocyte necrosis, perivenular fibrosis, pseudolobule formation, and mild lymphocytic infiltration. Pathological changes were alleviated to varying degrees in the treatment groups.

Additionally, as depicted in Fig. 1B-C, the levels of ALT and AST were markedly increased in the model group after exposure to CCl_4. In the treatment groups, the rise in ALT levels was significantly suppressed, while AST levels showed a decreasing trend. These findings indicate that PHI and FA effectively mitigate CCl_4-induced hepatic injury in mice.

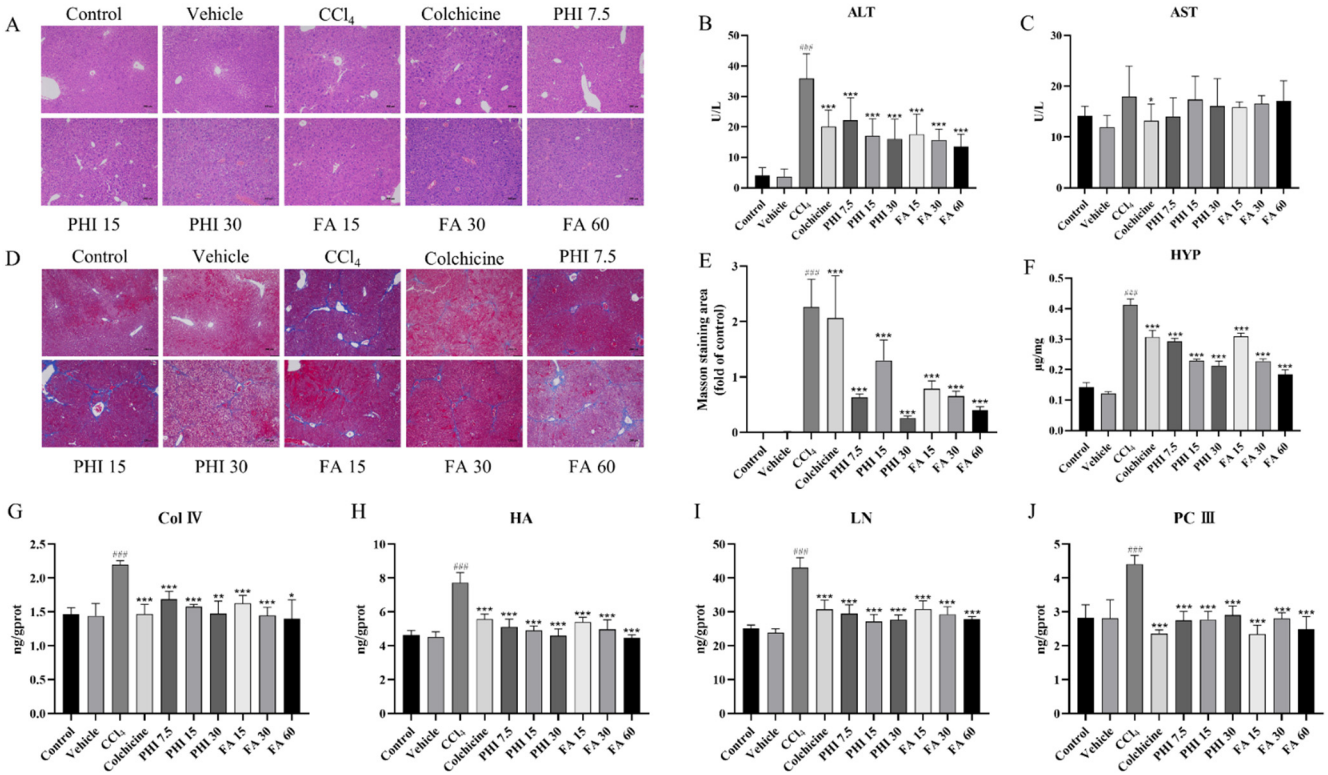

Fig. 1. PHI and FA ameliorated hepatic pathological alterations and enhanced liver function parameters. (A) HE staining results of mice in each group at week 5. (B-C) Quantification of ALT and AST levels in serum determined with assay kits (n=6). (D) Results of Masson staining in mice from each experimental group at week 5. (E) Quantitative analysis of Masson staining (n=3). (F) HYP levels in hepatic tissues from each group (n=6). (G-J) Levels of liver fibrosis markers (Col IV, HA, LN, and PC III) in liver tissues of each group. Results are presented as mean ± SD. $^{\#\#\#}P < 0.001$ vs Control group; $^{*}P < 0.05$, $^{**}P < 0.01$, $^{***}P < 0.001$ vs CCl_4 group.

3.1.2. PHI and FA decreased collagen accumulation and lowered the fibrosis index

Collagen, the primary structural protein in fibrotic tissues, critically contributes to liver fibrosis. Masson staining was utilized to examine collagen deposition as a means of evaluating liver fibrosis progression. As Fig. 1D demonstrated, blue-stained collagen fibers revealed substantial accumulation in CCl_4 model group,

whereas control groups showed minimal deposition. Treatment with PHI and FA significantly suppressed collagen fiber expression.

In addition, Col IV, HA, LN, and PC III are well-established markers that are highly expressed in those affected by liver fibrosis. For additional assessment of fibrosis severity, we determined the concentrations of these markers. As illustrated in Fig. 1G-J, Col IV, HA, LN, and PC III levels were markedly increased in the CCl_4 model group relative to the control group. Nevertheless, PHI and FA treatments led to a significant decrease in the expression of these markers. Consistent with these observations, hepatic HYP levels, a direct fibrosis marker, were also decreased (Fig. 1F), aligning with the suppression of other fibrosis markers. Collectively, these experiments demonstrate that PHI and FA can effectively ameliorate CCl_4-induced liver fibrosis in mice.

3.1.3. PHI and FA inhibited HSC activation

Activation of HSCs, the primary ECM producers, is a hallmark of liver fibrosis. α-SMA serves as a biomarker for HSC activation, and COL-I is a significant ECM element. Immunohistochemistry was employed to evaluate the expression of α-SMA and COL-I in liver tissues (Fig. 2A-B). The findings revealed a marked elevation in α-SMA and COL-I expression in the CCl_4 model group. PHI and FA administration dose-dependently attenuated both markers, demonstrating effective suppression of HSC activation during liver fibrosis.

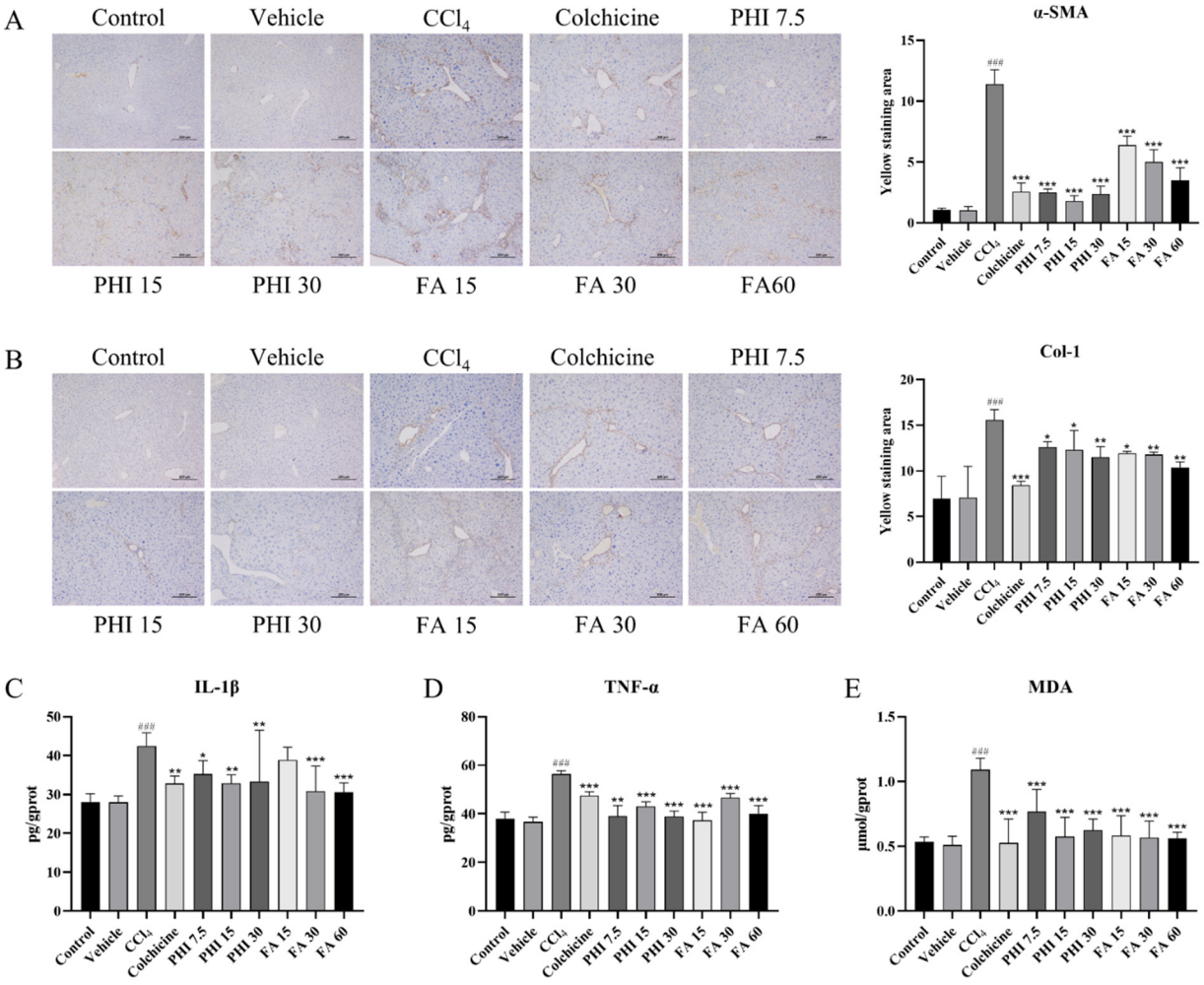

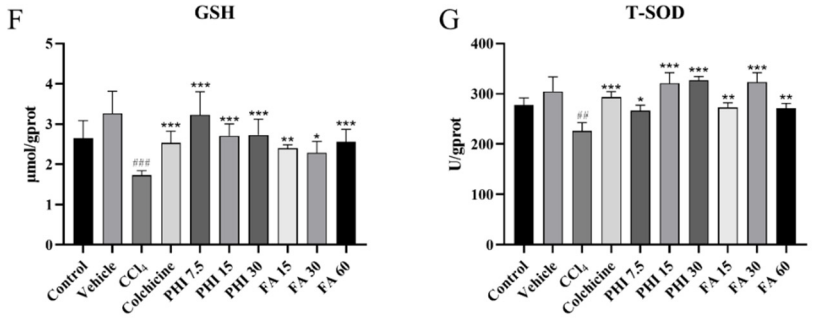

Fig. 2. PHI and FA inhibited HSC activation, inflammation, and oxidative stress damage. (A) α-SMA expression in liver tissues was assessed through immunohistochemical staining and quantitative analysis (n=3). (B) COL-I expression in liver tissues was assessed through immunohistochemical staining and quantitative analysis (n=3). (C-D) Changes in the expression levels of inflammatory cytokines IL-1β and TNF-α in liver tissues (n=6). (E-G) Changes in oxidative stress markers, including MDA, GSH, and T-SOD, in liver tissues (n=6). Results are presented as mean ± SD. $^{\#\#}P < 0.01$, $^{\#\#\#}P < 0.001$ vs Control group; $^{*}P < 0.05$, $^{**}P < 0.01$, $^{***}P < 0.001$ vs CCl_4 group.

3.1.4. PHI and FA inhibited inflammation and oxidative stress damage.

Further evaluation was conducted to assess the influence of PHI and FA on pro-inflammatory cytokines and oxidative stress markers in mice with CCl_4-induced liver fibrosis. As shown in Fig. 2C-G, the CCl_4-induced model group exhibited significantly elevated inflammatory mediators (IL-1β, TNF-α) and oxidative stress markers (MDA), alongside depleted antioxidants (GSH, T-SOD). Treatment with PHI and FA effectively reversed these changes. These findings indicate that CCl_4-induced liver fibrosis in mice is associated with significant inflammation and oxidative stress, which can be effectively alleviated by PHI and FA.

3.2. PHI and FA inhibited LPS + ATP-induced LO2 cell injury

3.2.1. Effects of PHI and FA on LO2 cell viability

LO2 cell viability was assessed by MTT assay under varying PHI/FA concentrations. As depicted in Fig. 3A, PHI did not significantly impact LO2 cell growth at concentrations ranging from 5 to 40 μg/mL. However, cell viability was significantly inhibited when the PHI concentration exceeded 40 μg/mL. Similarly, Fig. 3B demonstrated the influence of FA on LO2 cell viability. FA did not affect cell growth within the concentration range of 6.25-150 μg/mL, but a significant reduction in viability was observed at concentrations above 150 μg/mL. Based on these findings, safe concentrations of 10, 20, and 40 μg/mL for PHI and 37.5, 75, and 150 μg/mL for FA were selected for subsequent experiments.

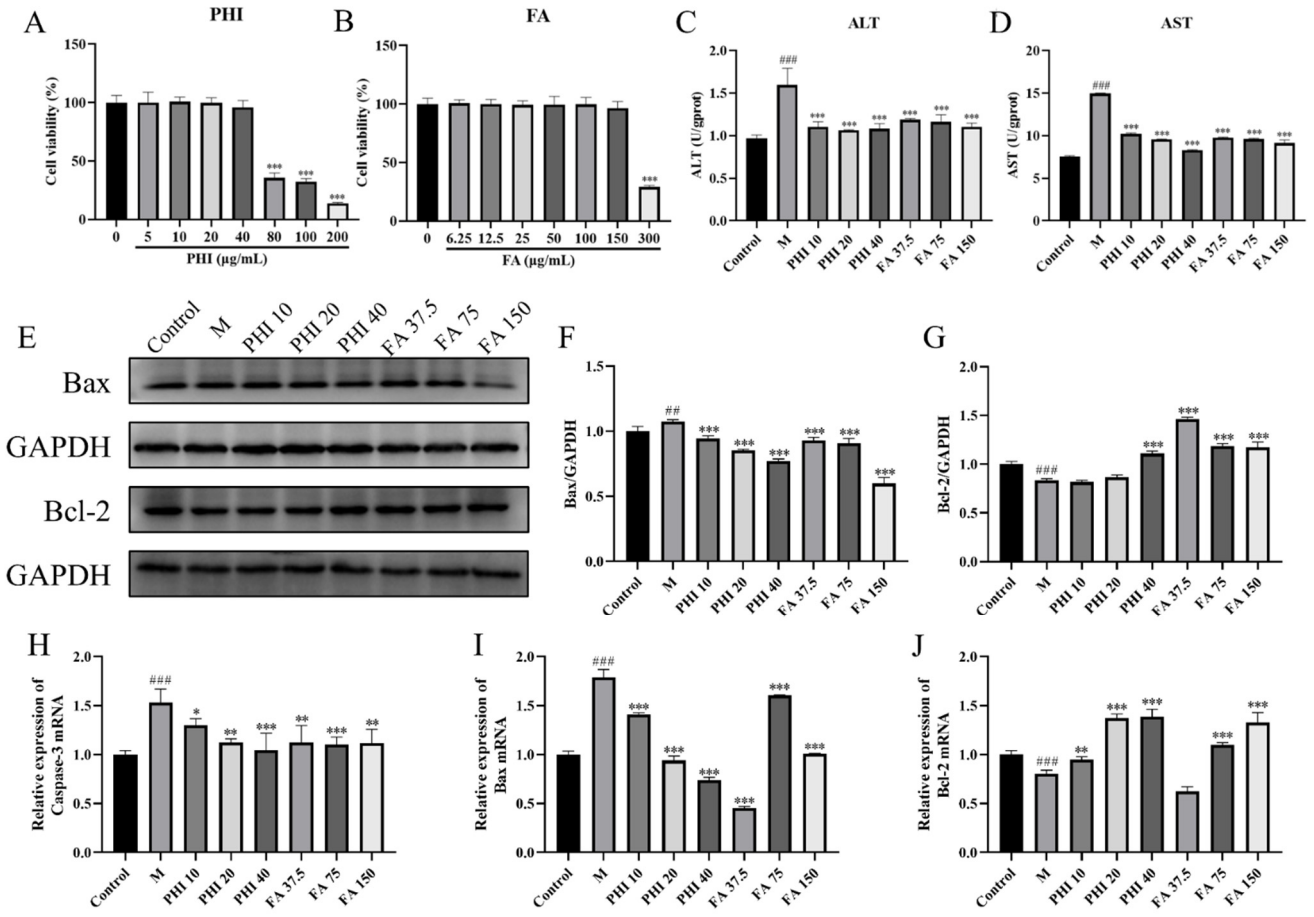

Fig. 3. Effects of PHI and FA on LO2 cell viability and apoptosis. (A) MTT assay results showing the effects of different concentrations of PHI on LO2 cell viability (n=6). (B) MTT assay results showing the effects of different concentrations of FA on LO2 cell viability (n=6). Results are presented as mean ± SD. $^{***}P < 0.001$ vs Control group. (C) Serum ALT levels in LO2 cells after modeling and treatment, as detected by assay kits (n=3). (D) Serum AST levels in LO2 cells after modeling and treatment, as detected by assay kits (n=3). (E) Western blot analysis of Bax and Bcl-2 protein expression in LO2 cells after modeling and treatment. (F-G) Relative quantification of Bax and Bcl-2 protein expression based on Western blot results, analyzed using ImageJ software (n=3). (H-J) RT-qPCR analysis of Caspase-3, Bax, and Bcl-2 mRNA expression in LO2 cells after modeling and treatment (n=3). Results are presented as mean ± SD. $^{\#\#}P < 0.01$, $^{\#\#\#}P < 0.001$ vs Control group; $^{*}P < 0.05$, $^{**}P < 0.01$, $^{***}P < 0.001$ vs M group.

3.2.2. Effects of PHI and FA on the expression of apoptosis-related markers in LO2 cells

Earlier research has demonstrated that hepatocyte apoptosis is crucial in the development of liver fibrosis[27]. To further explore the antifibrotic mechanisms of PHI and FA, we examined apoptosis-related markers. First, liver injury markers ALT and AST were measured in LO2 cells following modeling and treatment using assay kits. As depicted in Fig. 3C-D, ALT and AST levels were markedly higher in the model group than in the control group. PHI or FA treatment led to a significant decrease in ALT and AST levels relative to the model group. Next, we investigated the effects of PHI and FA on the expression of apoptosis-related markers in LO2 cells. As revealed by Western blot analysis, LPS + ATP treatment significantly increased Bax expression while reducing Bcl-2 levels. PHI or FA treatment reversed these effects (Fig. 3E-G). Similarly, RT-qPCR showed LPS + ATP treatment markedly increased mRNA levels of pro-apoptotic markers Caspase-3 and Bax while decreasing anti-apoptotic Bcl-2 mRNA, alterations significantly counteracted by PHI and FA (Fig. 3H-J).

3.2.3. Effects of PHI and FA on oxidative stress in LO2 cells

Earlier research has shown that oxidative stress is a key factor in the development of liver fibrosis[28]. To evaluate the antioxidant effects of PHI and FA, we first measured superoxide dismutase (SOD) expression in LO2 cells following modeling and treatment using assay kits. SOD levels were significantly reduced in model group versus control group (Fig. 4A), whereas PHI/FA treatments substantially reversed the decrease in SOD. To further investigate the antioxidant mechanisms of PHI and FA, we examined the classical Nrf2/HO-1 antioxidant signaling pathway. Mechanistic investigation revealed that LPS + ATP downregulated Nrf2/HO-1 protein expression (Fig. 4B-D) and corresponding mRNA levels (Fig. 4E-F), whereas PHI/FA potently reactivated this cytoprotective pathway. These results suggest that PHI and FA alleviate LPS + ATP-induced oxidative stress damage in hepatocytes by activating the Nrf2/HO-1 signaling pathway.

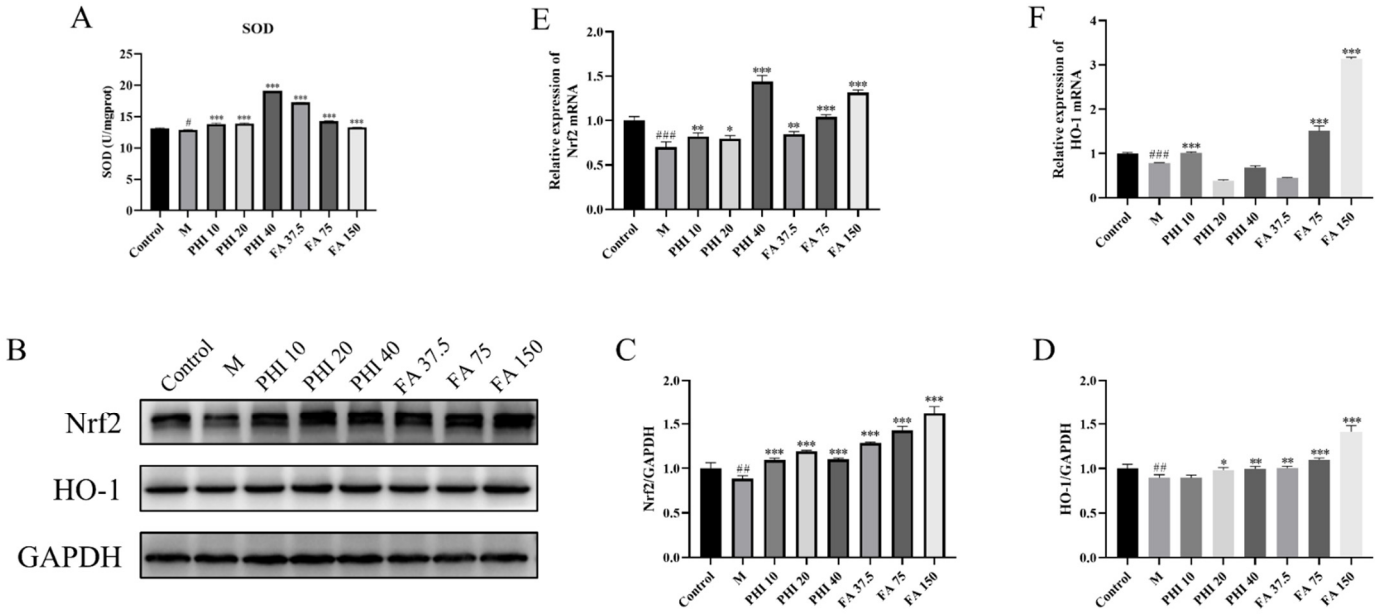

Fig. 4. Effects of PHI and FA on oxidative stress in LO2 cells. (A) SOD expression in LO2 cells after modeling and treatment, as detected by assay kits (n=3). (B) Western blot analysis of Nrf2 and HO-1 protein expression in LO2 cells after modeling and treatment. (C-D) Relative quantification of Nrf2 and HO-1 protein expression from Western blot results, analyzed using ImageJ software (n=3). (E-F) RT-qPCR analysis of Nrf2 and HO-1 mRNA expression in LO2 cells after modeling and treatment (n=3). Results are presented as mean ± SD. $^{\#}P < 0.05$, $^{\#\#}P < 0.01$, $^{\#\#\#}P < 0.001$ vs Control group; $^{*}P < 0.05$, $^{**}P < 0.01$, $^{***}P < 0.001$ vs M group.

3.2.4. Effects of PHI and FA on inflammatory in LO2 cells

The progression of liver fibrosis has been demonstrated to be critically mediated by inflammatory cascade activation[22]. In order to assess the impact of PHI and FA on inflammatory responses, our initial step involved quantifying the concentrations of key pro-inflammatory mediators, namely TNF-α, IL-1β, and IL-6, in the extracellular fluid of LO2 cell through ELISA kits. As shown in Fig. 5A-C, TNF-α, IL-1β, and IL-6 concentrations were significantly elevated in the model group versus controls. PHI or FA treatment dose-dependently reduced these cytokines. In an effort to elucidate the molecular basis underlying the anti-inflammatory properties of PHI and FA in LO2 cells, we conducted a comprehensive investigation of the NLRP3 inflammasome signaling cascade. Western blot analysis revealed that LPS + ATP treatment significantly increased the protein expression levels of P2X7, NLRP3, TLR4, and NOX4. These increases

were markedly attenuated by treatment with PHI or FA (Fig. 5E-H). Consistent with these findings, RT-qPCR assays revealed that co-stimulation with LPS and ATP markedly enhanced transcriptional activity of P2X7, NLRP3, TLR4, and NOX4 genes. Conversely, therapeutic intervention with either PHI or FA demonstrated a substantial suppressive effect on the expression profiles of these molecular targets, as shown in Fig. 5I-L. These results indicate that PHI and FA mitigate LPS + ATP-induced inflammatory damage in hepatocytes by modulating the NLRP3-related signaling pathway.

3.3. PHI and FA inhibited LX2 cell activation and THP1 cell polarization via LO2 cell-derived exosomes

3.3.1. Characterization of LO2 cell-derived exosomes

The characterization of LO2 cell-derived exosomes is presented in Fig. 6A-B. Ultrastructural examination through TEM demonstrated the distinct spherical architecture typical of exosomal vesicles. The mean hydrodynamic diameter and quantitative profile of exosomal particles derived from the control (C-Exo), model (M-Exo), PHI-treated (PHI-Exo), and FA-treated (FA-Exo) groups were 79.0 nm, 2.06 × 10^{10} particles/mL; 76.7 nm, 1.29 × 10^{10} particles/mL; 83.6 nm, 3.75 × 10^{10} particles/mL; and 72.3 nm, 2.41 × 10^{10} particles/mL, respectively. Western blot confirmed positive expression of exosomal markers CD9/CD81 in all groups, with absence of the negative marker calnexin (Fig. 6C). These findings confirm that exosomes were successfully isolated from LO2 cells in this experiment.

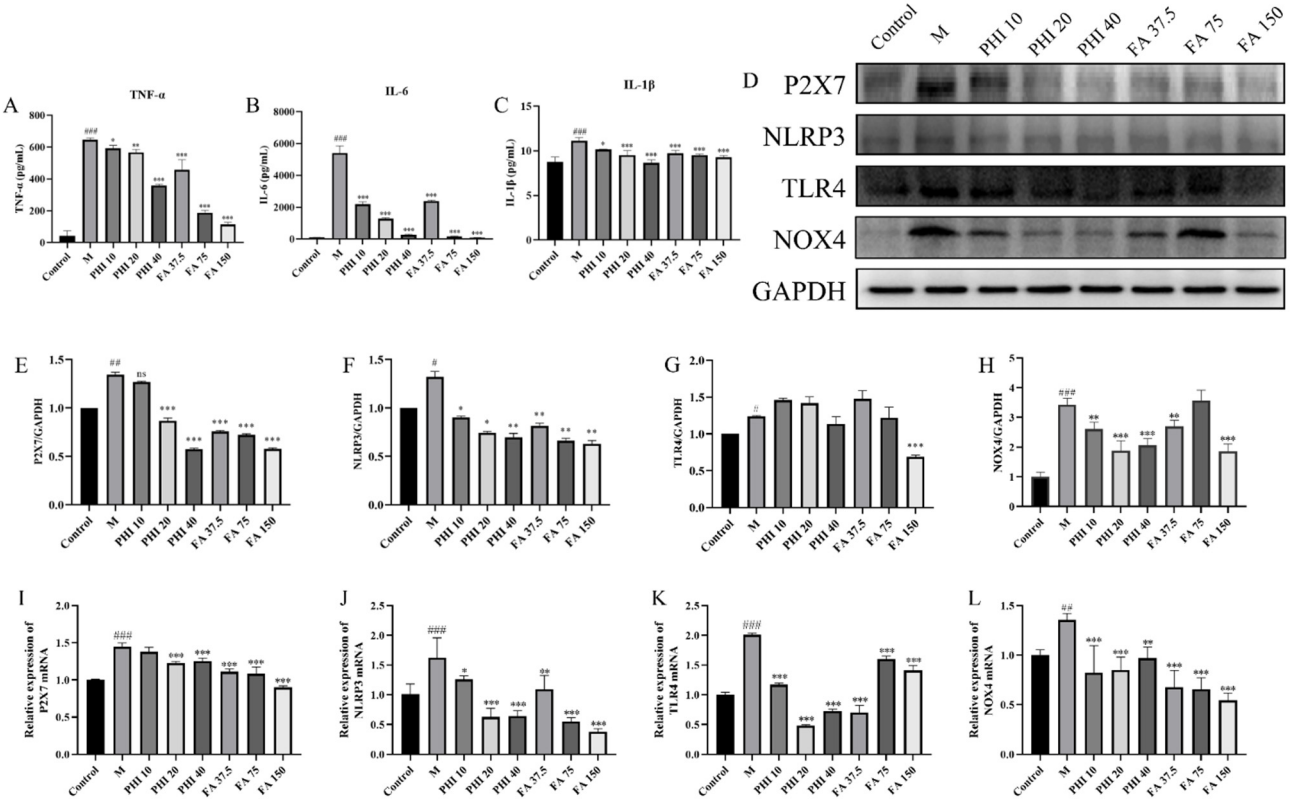

Fig. 5. Effects of PHI and FA on inflammatory in LO2 cells. (A-C) ELISA results showing the expression levels of TNF-α, IL-6, and IL-1β in the culture supernatants of LO2 cells (n=3). (D) Western blot analysis of P2X7, NLRP3, TLR4, and NOX4 protein expression in LO2 cells after modeling and treatment. (E-H) Relative quantification of P2X7, NLRP3, TLR4, and NOX4 protein expression based on Western blot results, analyzed using ImageJ software (n=3). (I-L) RT-qPCR results showing the mRNA expression levels of P2X7, NLRP3, TLR4, and NOX4 in LO2 cells after modeling and treatment (n=3). Results are presented as mean ± SD. $^{\#}P < 0.05$, $^{\#\#}P < 0.01$, $^{\#\#\#}P < 0.001$ vs Control group; $^{*}P < 0.05$, $^{**}P < 0.01$, $^{***}P < 0.001$ vs M group.

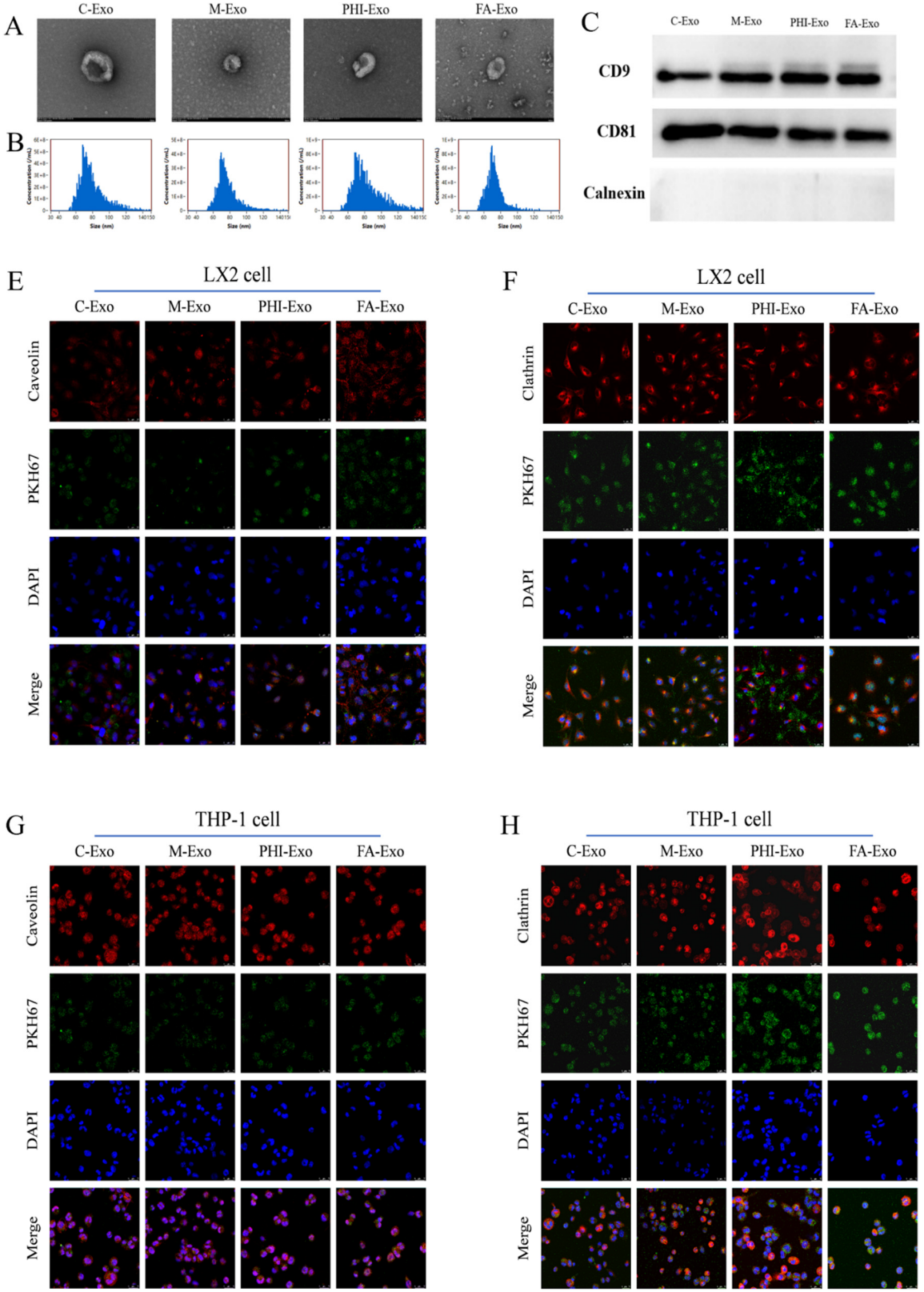

Fig. 6. Characterization and uptake mechanism of exosomes from different groups. (A) Morphology of C-Exo, M-Exo, PHI-Exo, and FA-Exo observed under transmission electron microscopy (TEM). (B) Particle size of C-Exo, M-Exo, PHI-Exo, and FA-Exo. (C) Western blot analysis of exosomal marker proteins CD9 and CD81, and the negative marker Calnexin, in C-Exo, M-Exo, PHI-Exo, and FA-Exo. (E) Immunofluorescence staining of Caveolin in LX2 cells after co-culture with LO2 cell-derived exosomes for 4 h. (F) Immunofluorescence staining of Clathrin in LX2 cells after co-culture with LO2 cell-derived exosomes for 4 h. (G) Immunofluorescence staining of Caveolin in THP1 cells after co-culture with LO2 cell-derived exosomes for 4 h. (H) Immunofluorescence staining of Clathrin in THP1 cells after co-culture with LO2 cell-derived exosomes for 4 h.

3.3.2. Uptake of LO2 cell-derived exosomes

The uptake of LO2 cell-derived exosomes is shown in Fig. 6E-H. Confocal microscopy was utilized to investigate the internalization of C-Exo, M-Exo, PHI-Exo, and FA-Exo by LX2 and THP1 cells, along with the colocalization of these exosomes with Caveolin and Clathrin proteins within the respective cellular contexts. Results revealed that both cell types internalized LO2 exosomes primarily via clathrin-mediated endocytosis.

3.3.3. Effects of LO2 cell-derived exosomes on LX2 cell activation

To investigate the effects of LO2 cell-derived exosomes on LX2 cell activation, LX2 cells were co-cultured with C-Exo, M-Exo, PHI-Exo, or FA-Exo. The expression levels of the activation markers α-SMA and HYP in LX2 cells were measured, along with the levels of inflammatory cytokines (IL-1β, IL-6, and TNF-α) in the culture supernatant. Additionally, oxidative stress markers SOD and MDA were evaluated. The experimental data presented in Fig. 7 demonstrated distinct molecular alterations in the M-Exo cohort relative to the C-Exo group, characterized by marked upregulation of fibrotic markers (α-SMA and HYP) and oxidative stress indicator (MDA), concomitant with suppression of the antioxidant enzyme SOD and substantial elevation in pro-inflammatory mediators (TNF-α, IL-6, and IL-1β). Crucially, PHI-Exo and FA-Exo treatments significantly reversed these pathological changes, indicating that PHI and FA exert their therapeutic effects by regulating HSC activation through exosomal signaling originating from LO2 cells, while concurrently demonstrating potent anti-inflammatory and antioxidant properties in LX2 cell cultures.

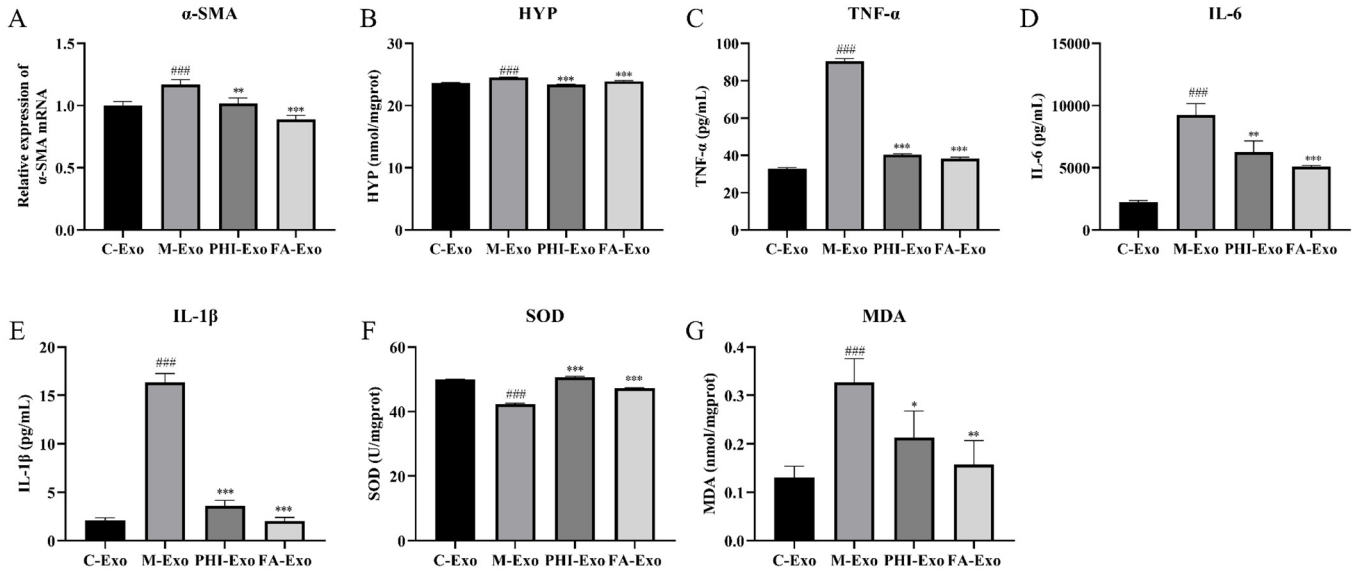

Fig. 7. PHI and FA regulated HSCs activation via LO2 cell-derived exosomes. (A) RT-qPCR analysis of α-SMA mRNA expression in LX2 cells after 24-hour co-culture with LO2 cell-derived exosomes under different treatments (n=3). (B) HYP expression in LX2 cells after 4-hour co-culture with LO2 cell-derived exosomes under different treatments, measured using an HYP assay kit (n=3). (C-E) ELISA analysis of TNF-α, IL-6, and IL-1β levels in LX2 cells after 24-hour co-culture with LO2 cell-derived exosomes under different treatments (n=3). (F-G) SOD and MDA levels in LX2 cells after 24-hour co-culture with LO2 cell-derived exosomes under different treatments, measured using respective assay kits (n=3). Results are presented as mean ± SD. $^{###}P < 0.001$ vs C-Exo group; $^{*}P < 0.05$, $^{**}P < 0.01$, $^{***}P < 0.001$ vs M-Exo group.

3.3.4. Effects of LO2 cell-derived exosomes on THP1 cell polarization

Following a 48-hour PMA treatment to initiate monocyte-to-macrophage differentiation, THP1-derived M0 macrophages were established and subsequently subjected to co-culture conditions with exosomes isolated from LO2 cells. Quantitative analysis of the culture medium revealed key biological mediators, including pro-inflammatory factors (IL-1β, IL-6, and TNF-α), redox status indicators (SOD and MDA), and characteristic M1 phenotype surface markers (CD71 and CD36). The experimental data presented in Fig. 8 demonstrated that M-Exo-treated THP1 cells exhibited distinct alterations versus the C-Exo group, including elevated pro-inflammatory cytokine secretion, increased MDA levels, suppressed SOD activity, and upregulated M1 marker expression (CD36/CD71). Importantly, these pathological alterations were substantially attenuated through therapeutic intervention with either PHI-Exo or FA-Exo. These results suggest that PHI and FA regulate macrophage polarization via LO2 cell-derived exosomes, thereby mitigating inflammation and oxidative stress in macrophages.

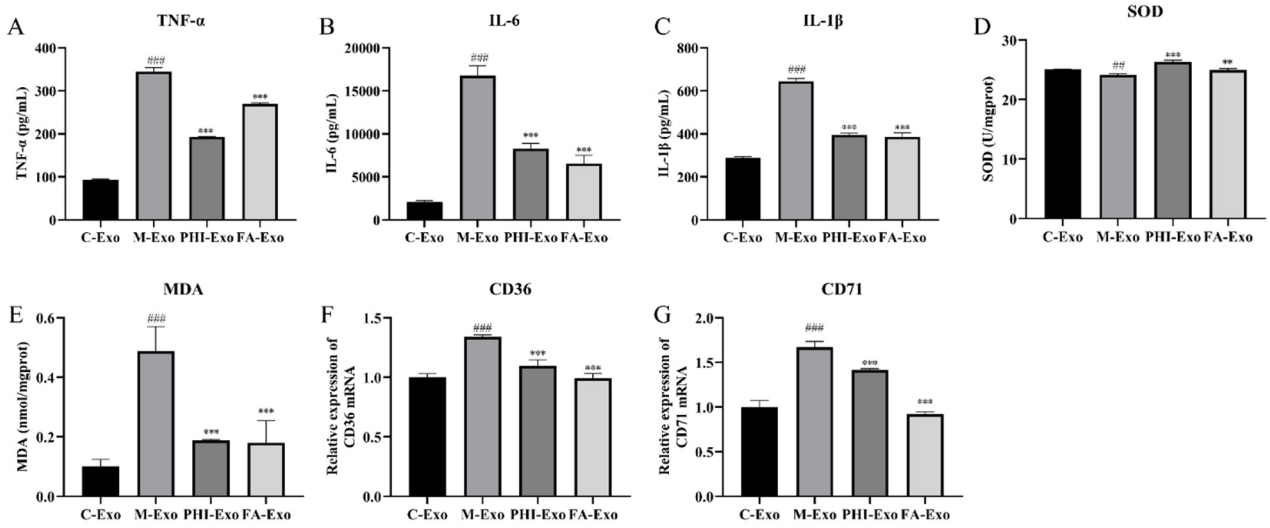

Fig. 8. PHI and FA regulated M1 polarization of M0 macrophages via LO2 cell-derived exosomes. (A-C) ELISA analysis of TNF-α, IL-6, and IL-1β levels in the culture supernatant of M0 macrophages co-cultured with LO2 cell-derived exosomes under different treatments for 24 hours (n=3). (D-E) SOD and MDA levels in M0 macrophages co-cultured with LO2 cell-derived exosomes under different treatments for 24 hours, measured using respective assay kits (n=3). (F-G) RT-qPCR analysis of CD36 and CD71 mRNA expression in M0 macrophages co-cultured with LO2 cell-derived exosomes under different treatments for 24 hours (n=3). Results are presented as mean ± SD. $^{\#\#}P < 0.01$, $^{\#\#\#}P < 0.001$ vs C-Exo group; $^{**}P < 0.01$, $^{***}P < 0.001$ vs M-Exo group.

3.3.5. Effects of LO2 cell-derived exosomes on LX2 and THP1 cells after endocytosis inhibition

To further elucidate the mechanism of exosome uptake in THP1 and LX2 cells, the clathrin-mediated endocytosis inhibitor Pitstop2 was employed. The experimental results depicted in Fig. 9 demonstrated that pharmacological inhibition with Pitstop2 differentially attenuated LO2-derived exosome effects on pro-inflammatory cytokines (IL-6, IL-1β, TNF-α) and SOD expression in both cell types. These findings suggested that the uptake of LO2 cell-derived exosomes by THP1 and LX2 cells is predominantly mediated through an endocytosis-dependent pathway.

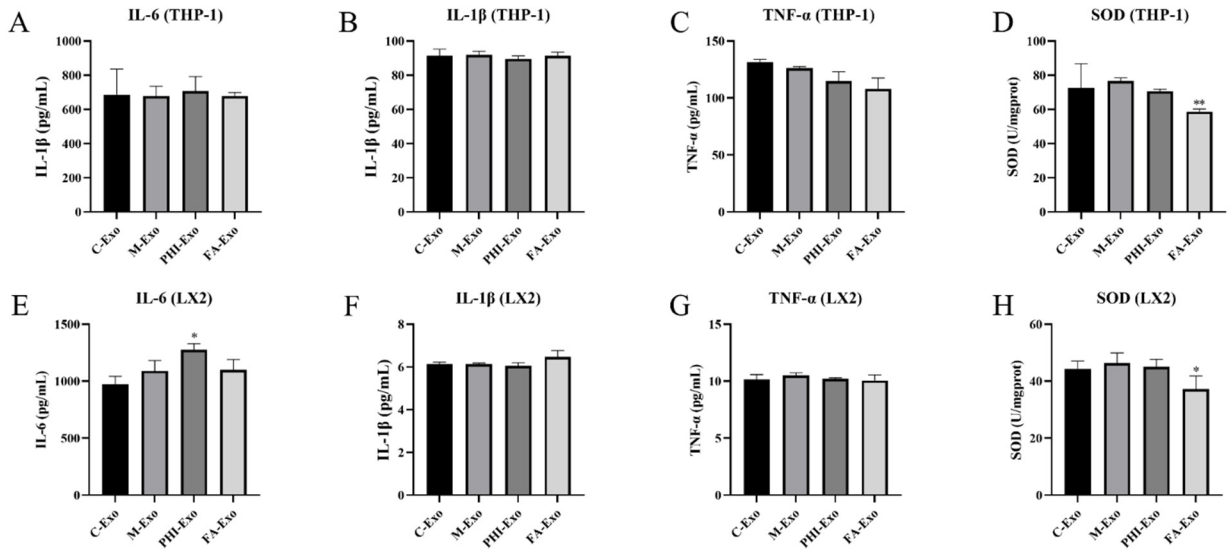

Fig. 9. Effects of endocytosis inhibition on IL-1β expression in THP1 and LX2 cells treated with LO2 cell-derived exosomes. (A-D) ELISA analysis of IL-6, IL-1β, TNF-α and SOD expression in THP1 cells treated with LO2 cell-derived exosomes after endocytosis inhibition using Pitstop2 (n=3). (B) ELISA analysis of IL-6, IL-1β, TNF-α and SOD expression in LX2 cells treated with LO2 cell-derived exosomes after endocytosis inhibition using Pitstop2 (n=3). Results are presented as mean ± SD. $^{*}P < 0.05$, $^{**}P < 0.01$ vs M-Exo group.

4. Discussion

Liver fibrosis represents a progressive pathological condition marked by abnormal ECM deposition, triggered by persistent hepatic damage stemming from multiple pathological mechanisms[2], such as programmed cell death[27], oxidative stress[28], and inflammation[22, 29, 30]. Persistent fibrosis may advance to irreversible cirrhosis or hepatocellular carcinoma (HCC)[6], highlighting the need for effective interventions. Activated HSCs and the dysregulation of M1/M2 macrophage polarization dynamics are central drivers of this pathology[1, 12]. Following hepatic damage, quiescent HSCs transition into myofibroblasts, exhibiting upregulated α-SMA and COL I expression while secreting inflammatory mediators, thereby driving fibrotic scar formation. The monocyte-derived immune cells primarily exist in two distinct polarization states: pro-inflammatory M1 phenotype and anti-inflammatory M2 phenotype. The pro-inflammatory M1 phenotype secretes key inflammatory mediators including IL-6 and TNF-α, thereby exacerbating hepatic inflammatory responses and tissue injury[25, 31]. Conversely, the anti-inflammatory M2 phenotype produces regulatory cytokines including IL-10 and TGF-β, which mediate tissue regeneration and promote hepatic recovery processes[24]. The dysregulation of M1/M2 macrophage polarization dynamics significantly influences both the development and resolution of hepatic fibrotic processes. As a result, suppressing HSC activation and M1 macrophage polarization has emerged as a promising therapeutic strategy for treating liver fibrosis. In previous studies, PHI was found to suppress M1 macrophage polarization by inhibiting the JAK1/JAK2-STAT1 and Notch1 signaling pathways[31], and to inhibit LX2 cell activation via the TLR4/MyD88/NF-κB signaling axis[32]. Similarly, FA has been demonstrated to attenuate LX2 cell activation through extracellular matrix remodeling and amelioration of oxidative imbalance[12]. However, the precise mechanisms underlying the cellular actions of FA and PHI remain incompletely understood. Therefore, this

study was designed to investigate whether their mechanisms involve exosome-mediated intercellular communication. Accordingly, exosomes were isolated from the supernatant of PHI- or FA-treated LO2 cells using differential ultracentrifugation. During this isolation procedure, the supernatant was processed with 100-kDa molecular weight cutoff ultrafiltration devices to effectively eliminate residual free PHI and FA drugs, thereby eliminating potential direct effects of PHI and FA on LX2 and THP-1 cells. Subsequently, comprehensive characterization and functional validation were performed on the isolated exosome preparations to confirm successful purification of exosomes.

Crucially, our study reveals a novel exosome-mediated mechanism that hepatocytes subjected to inflammatory stimuli (LPS/ATP) secrete exosomes (M-Exo) that promote LX2 cell activation and M1 polarization of macrophages. Conversely, exosomes from PHI/FA-pretreated LO2 cells (PHI-Exo/FA-Exo) reverse these profibrotic effects, indicating PHI/FA reprogram hepatocyte exosome cargo to exert antifibrotic actions. In this study, we used methods established based on previous research to extract and isolate exosomes, and rigorously characterized the isolates through various methods[31, 33, 34]. We performed TEM showing typical cup-shaped morphology, western blot for exosomal markers (e.g., CD63, TSG101) and absence of negative markers (e.g., calnexin), NTA demonstrating a particle size distribution peaking at 50-150 nm. These data collectively support that our isolation method effectively minimized contamination from other EVs or cellular debris. The exosomes used for functional assays were administered at a concentration of 10 μg/mL based on our previously established protocols. In previous studies, we treated macrophages with PHI and isolated the resulting exosomes (PHI-Exo), which were diluted to a concentration of 10 μg/mL in fresh culture medium and co-cultured with mHSCs. The results demonstrated that PHI-Exo significantly attenuated the activation of hepatic stellate cells. Our previous research also employs FA-loaded exosome concentrations ranging from 3.75 to 60 μg/mL in vitro models, which effectively elicit detectable biological responses while avoiding overt cytotoxicity[31, 33]. Prior studies have demonstrate that clathrin inhibition (via Pitstop2 or siRNA) significantly blocks exosome uptake in similar cell types. For instance, it has been demonstrated that the clathrin-dependent endocytosis inhibitor Pitstop2 suppresses cellular albumin uptake[35], and genetic ablation of the key endocytosis gene clathrin heavy chain (Cltc) markedly reduces exosome uptake by macrophages both *in vitro* and *in vivo*[36]. Furthermore, our study observed colocalization of exosomes with clathrin and demonstrated that pharmacological inhibition using Pitstop2, a clathrin-mediated endocytosis inhibitor, significantly attenuated the exosome-induced modulatory effects on cytokine/SOD expression profiles. These findings suggest that the clathrin-mediated endocytic pathway may play an important role in both the uptake of LO2 cell-derived exosomes by LX2/THP1 cells and the subsequent functional outcomes mediated by these exosomes. However, the reliance on a single pharmacological inhibitor represents a methodological limitation. Consequently, future studies will systematically compare multiple pathways (e.g., using dynamin mutants or pathway-specific siRNA).

Exosome cargos are composed of DNA, proteins, lipid cargo, metabolites, mRNA, and non-coding RNA, and plays an important role in the development of liver fibrosis[37]. Previous studies have demonstrated that

PHI suppresses HSC activation by inhibiting miR-125b-5p expression in exosomes derived from M1 macrophages[31]. Furthermore, exosomes delivering obeticholic acid attenuate hepatic fibrogenesis by inhibiting HSC activation and modulating ECM remodeling[38]. In the present study, PHI/FA pretreatment significantly regulates the expression of inflammation and antioxidant related factors in LO2 cells, suggesting that it may selectively enrich exosomes with anti-inflammatory or antioxidant activity by reshaping the cell secretion group. The biological effects of exosomes, such as inhibition of IL-1β and enhancement of SOD, depend on the endocytic pathway of receptor cells, indicating that their action is mediated by content delivery rather than membrane surface contact. Therefore, we speculate that exosomes may carry regulatory molecules such as miRNAs targeting the anti-inflammatory proteins or antioxidant enzymes. Future studies will employ exosomal miRNA sequencing and proteomics to identify and validate these core effector molecules, thereby addressing the current mechanistic gap.

In recent years, exosomes have garnered extensive exploration in the biomedical field, particularly concerning liver fibrosis, owing to their favorable biocompatibility, suitable size, and low immunogenicity. Exosomes demonstrate significant diagnostic potential for liver fibrosis. For instance, serum-derived exosomal miR-92a-3p and miR-146a-5p show promise as biomarkers for assessing chronic hepatitis B progression[39]. Furthermore, exosomes hold therapeutic potential as therapeutic agents[40], therapeutic targets[41] or drug delivery systems[33] for treating liver fibrosis. This study highlights the antifibrotic potential of PHI and FA from *Forsythia suspensa*, mediated via LO2 cell-derived exosomes, in suppressing HSC activation and macrophage M1 polarization. These findings indicate that PHI and FA may exert antifibrotic effects by modulating hepatocyte exosome-mediated intercellular communication, offering a novel therapeutic strategy for liver fibrosis intervention.

5. Conclusion

As shown in Fig. 10, we demonstrated that PHI and FA improve hepatocyte injury by inhibiting apoptosis, oxidative stress, and inflammatory responses through multiple pathways. Additionally, PHI and FA suppress HSC activation and macrophage polarization via LO2 cell-derived exosomes, thereby alleviating liver fibrosis. This study enhances our understanding of the interactions between hepatocytes, HSCs, and macrophages, further elucidating the mechanisms through which PHI and FA inhibit liver fibrosis. It provides a theoretical basis for exploring the antifibrotic mechanisms of Forsythiae Fructus, offering valuable insights for future research and the development of antifibrotic therapies.

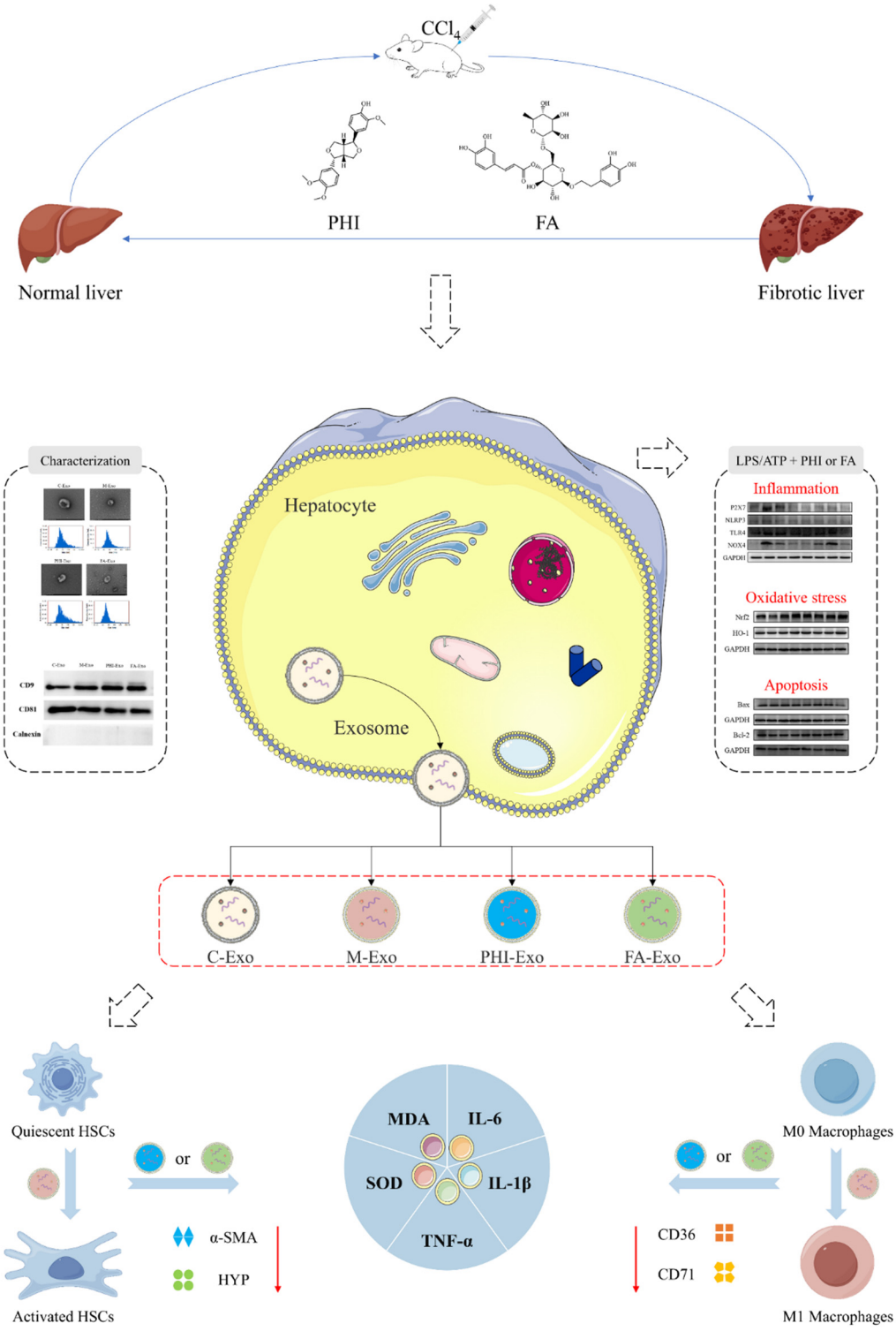

Fig. 10. Schematic representation of the effects of PHI and FA on hepatic stellate cells and macrophages via hepatocyte-derived exosomes.

Acknowledgements

This work was supported by the National Natural Science Foundation of China (No: U24A20790), Innovation Fund of the Chengdu Municipal Health Commission and Higher Education Institutions (WXLH202402028), Innovation Team and Talents Cultivation Program of National Administration of Traditional Chinese Medicine (No: ZYYCXTD-D-202209), Sichuan TCM Science and Technology Industry Innovation Team (No: 2022C001).

Declaration of competing interest

All the authors claimed that there was no conflict of interest.

Data Availability Statement

The data that support the findings of this study are available from the corresponding author upon reasonable request.

References

[1] H. Rho, A.R. Terry, C. Chronis, et al., Hexokinase 2-mediated gene expression via histone lactylation is required for hepatic stellate cell activation and liver fibrosis, Cell Metab. 35 (2023) 1406-1423.e1408. https://doi.org/10.1016/j.cmet.2023.06.013.

[2] M. Parola, M. Pinzani, Liver fibrosis: Pathophysiology, pathogenetic targets and clinical issues, Mol. Asp. Med. 65 (2019) 37-55. https://doi.org/10.1016/j.mam.2018.09.002.

[3] M.A. Abdel-Wahhab, A.A. El-Nekeety, M.A. Hassan, et al., Casein or soy protein supplementation protects against hepatotoxicity in hypercholesterolemic rats treated with rosuvastatin, Food & Medicine Homology. (2025) https://doi.org/10.26599/FMH.2026.9420088.

[4] J. Dong, B.-D. Zhang, S. Li, et al., Identification of sesquiterpenes from Curcuma longa and its potential for alcoholic liver disease based on FBMN strategy and network pharmacology, Food & Medicine Homology. (2025) https://doi.org/10.26599/FMH.2026.9420114.

[5] L. Guo, Q.-Y. Ding, W.-H. Duan, et al., Goji-Derived Exosomes-Like Nanoparticles Ameliorate Alcohol-Induced Acute Liver Injury by modulating gut microbiota and metabolites, Food & Medicine Homology. (2025) https://doi.org/10.26599/FMH.2026.9420081.

[6] M. Sun, T. Kisseleva, Reversibility of liver fibrosis, Clin. Res. Hepatol. Gastroenterol. 39 Suppl 1 (2015) S60-63. https://doi.org/10.1016/j.clinre.2015.06.015.

[7] N. Hu, C. Guo, X. Dai, et al., Forsythiae Fructuse water extract attenuates liver fibrosis via TLR4/MyD88/NF-κB and TGF-β/smads signaling pathways, J. Ethnopharmacol. 262 (2020) https://doi.org/10.1016/j.jep.2020.113275.

[8] Z. Wang, Q. Xia, X. Liu, et al., Phytochemistry, pharmacology, quality control and future research of Forsythia suspensa (Thunb.) Vahl: A review, J. Ethnopharmacol. 210 (2018) 318-339. https://doi.org/10.1016/j.jep.2017.08.040.

[9] K. Fu, C. Ma, C. Wang, et al., Forsythiaside A alleviated carbon tetrachloride-induced liver fibrosis by modulating gut microbiota composition to increase short-chain fatty acids and restoring bile acids metabolism disorder, Biomed. Pharmacother. 151 (2022) https://doi.org/10.1016/j.biopha.2022.113185.

[10] C. Wang, Y. Liu, L. Gong, et al., Phillygenin Ameliorates Carbon Tetrachloride-Induced Liver Fibrosis: Suppression of Inflammation and Wnt/β-Catenin Signaling Pathway, Inflammation. 46 (2023) 1543-1560. https://doi.org/10.1007/s10753-023-01826-1.

[11] C. Wang, C. Ma, K. Fu, et al., Phillygenin Attenuates Carbon Tetrachloride-Induced Liver Fibrosis via Modulating Inflammation and Gut Microbiota, Front. Pharmacol. 12 (2021) https://doi.org/10.3389/fphar.2021.756924.

[12] M. Zhou, X. Zhao, L. Liao, et al., Forsythiaside A Regulates Activation of Hepatic Stellate Cells by Inhibiting NOX4-Dependent ROS, Oxidative Med. Cell. Longev. 2022 (2022) 1-17. https://doi.org/10.1155/2022/9938392.

[13] C. Wang, C. Ma, K. Fu, et al., Hepatoprotective effect of phillygenin on carbon tetrachloride-induced liver fibrosis and its effects on short chain fatty acid and bile acid metabolism, J. Ethnopharmacol. 296 (2022) 115478. https://doi.org/10.1016/j.jep.2022.115478.

[14] S. Cheng, Y. Zou, M. Zhang, et al., Single-cell RNA sequencing reveals the heterogeneity and intercellular communication of hepatic stellate cells and macrophages during liver fibrosis, MedComm. 4 (2023) https://doi.org/10.1002/mco2.378.

[15] S. Tian, X. Zhou, M. Zhang, et al., Mesenchymal stem cell-derived exosomes protect against liver fibrosis via delivering miR-148a to target KLF6/STAT3 pathway in macrophages, Stem Cell Res. Ther. 13 (2022) https://doi.org/10.1186/s13287-022-03010-y.

[16] M.E. Zahmatkesh, M. Jahanbakhsh, N. Hoseini, et al., Effects of Exosomes Derived From Helicobacter pylori Outer Membrane Vesicle-Infected Hepatocytes on Hepatic Stellate Cell Activation and Liver Fibrosis Induction, Front. Cell. Infect. Microbiol. 12 (2022) https://doi.org/10.3389/fcimb.2022.857570.

[17] X. Zhao, X. Xue, Z. Cui, et al., microRNAs-based diagnostic and therapeutic applications in liver fibrosis, Wiley Interdiscip. Rev.-RNA. 14 (2022) https://doi.org/10.1002/wrna.1773.

[18] S. Gurung, D. Perocheau, L. Touramanidou, et al., The exosome journey: from biogenesis to uptake and intracellular signalling, Cell Commun. Signal. 19 (2021) 47. https://doi.org/10.1186/s12964-021-00730-1.

[19] Q. Zhang, Y. Qu, Q. Zhang, et al., Exosomes derived from hepatitis B virus-infected hepatocytes promote liver fibrosis via miR-222/TFRC axis, Cell Biol. Toxicol. 39 (2022) 467-481. https://doi.org/10.1007/s10565-021-09684-z.

[20] L. Yang, Y.L. Gao, S. Jiang, et al., Aflatoxin B(1)-exposed hepatocyte-derived extracellular vesicles: Initiating hepatic stellate cell-mediated liver fibrosis through a p53-Parkin-dependent mitophagy pathway, Ecotoxicol. Environ. Saf. 277 (2024) 116363. https://doi.org/10.1016/j.ecoenv.2024.116363.

[21] Y.-j. Li, R.-p. Liu, M.-n. Ding, et al., Tetramethylpyrazine prevents liver fibrotic injury in mice by targeting hepatocyte-derived and mitochondrial DNA-enriched extracellular vesicles, Acta Pharmacol. Sin. 43 (2022) 2026-2041. https://doi.org/10.1038/s41401-021-00843-w.

[22] A. Wree, A. Eguchi, M.D. McGeough, et al., NLRP3 inflammasome activation results in hepatocyte pyroptosis, liver inflammation, and fibrosis in mice, Hepatology. 59 (2014) 898-910. https://doi.org/10.1002/hep.26592.

[23] G. Shu, A. Yusuf, C. Dai, et al., Piperine inhibits AML-12 hepatocyte EMT and LX-2 HSC activation and alleviates mouse liver fibrosis provoked by CCl(4): roles in the activation of the Nrf2 cascade and subsequent suppression of the TGF-β1/Smad axis, Food Funct. 12 (2021) 11686-11703. https://doi.org/10.1039/d1fo02657g.

[24] Y. Wang, S. Huang, W. Kong, et al., Corilagin alleviates liver fibrosis in zebrafish and mice by repressing IDO1-mediated M2 macrophage repolarization, Phytomedicine. 119 (2023) 155016. https://doi.org/10.1016/j.phymed.2023.155016.

[25] J. Zhang, Y. Liu, H. Chen, et al., MyD88 in hepatic stellate cells enhances liver fibrosis via promoting macrophage M1 polarization, Cell Death Dis. 13 (2022) https://doi.org/10.1038/s41419-022-04802-z.

[26] J. Kang, J. Postigo-Fernandez, K. Kim, et al., Notch-mediated hepatocyte MCP-1 secretion causes liver fibrosis, JCI insight. 8 (2023) https://doi.org/10.1172/jci.insight.165369.

[27] M. Jiang, C. Huang, Q. Wu, et al., Sini San ameliorates CCl4-induced liver fibrosis in mice by inhibiting AKT-mediated hepatocyte apoptosis, J. Ethnopharmacol. 303 (2023),

[28] S.E. Abu-Risha, S.S. Sokar, H.R. Elbohoty, et al., Combined carvacrol and cilostazol ameliorate ethanol-induced liver fibrosis in rats: Possible role of SIRT1/Nrf2/HO-1 pathway, Int. Immunopharmacol. 116 (2023),

[29] C. Rossi, A. Salvati, M. Distaso, et al., The P2X7R-NLRP3 and AIM2 Inflammasome Platforms Mark the Complexity/Severity of Viral or Metabolic Liver Damage, Int. J. Mol. Sci. 23 (2022) https://doi.org/10.3390/ijms23137447.

[30] Y. Nie, Q. Liu, W. Zhang, et al., Ursolic acid reverses liver fibrosis by inhibiting NOX4/NLRP3 inflammasome pathways and bacterial dysbiosis, Gut Microbes. 13 (2021) https://doi.org/10.1080/19490976.2021.1972746.

[31] C. Ma, C. Wang, Y. Zhang, et al., Phillygenin inhibited M1 macrophage polarization and reduced hepatic stellate cell activation by inhibiting macrophage exosomal miR-125b-5p, Biomed. Pharmacother. 159 (2023) https://doi.org/10.1016/j.biopha.2023.114264.

[32] N. Hu, C. Wang, X. Dai, et al., Phillygenin inhibits LPS-induced activation and inflammation of LX2 cells by TLR4/MyD88/NF-κB signaling pathway, J. Ethnopharmacol. 248 (2020) 112361. https://doi.org/10.1016/j.jep.2019.112361.

[33] L. Gong, H. Zhou, S. Zhang, et al., CD44-Targeting Drug Delivery System of Exosomes Loading Forsythiaside A Combats Liver Fibrosis via Regulating NLRP3-Mediated Pyroptosis, Advanced healthcare materials. 12 (2023) e2202228. https://doi.org/10.1002/adhm.202202228.

[34] L. Gong, H. Zhou, Y. Zhang, et al., Preparation of Phillygenin-Hyaluronic acid composite milk-derived exosomes and its anti-hepatic fibrosis effect, Materials today. Bio. 23 (2023) 100804. https://doi.org/10.1016/j.mtbio.2023.100804.

[35] H. Sun, Y.U. Takebayashi, H. Motohashi, et al., Internalization of FITC-albumin in Human Adipose-derived Stem Cells: Involvement of Clathrin and Caveolin, Die Pharmazie. 77 (2022) 141-146. https://doi.org/10.1691/ph.2022.2340.

[36] Z. Wan, L. Zhao, F. Lu, et al., Mononuclear phagocyte system blockade improves therapeutic exosome delivery to the myocardium, Theranostics. 10 (2020) 218-230. https://doi.org/10.7150/thno.38198.

[37] M. Babuta, G. Szabo, Extracellular vesicles in inflammation: Focus on the microRNA cargo of EVs in modulation of liver diseases, J Leukoc Biol. 111 (2022) 75-92. https://doi.org/10.1002/jlb.3mir0321-156r.

[38] A. Azizsoltani, B. Hatami, M.R. Zali, et al., Obeticholic acid-loaded exosomes attenuate liver fibrosis through dual targeting of the FXR signaling pathway and ECM remodeling, Biomed. Pharmacother. 168 (2023) 115777. https://doi.org/10.1016/j.biopha.2023.115777.

[39] Q. Wang, Q. Hu, Y. Ying, et al., Using Next-generation Sequencing to Identify Novel Exosomal miRNAs as Biomarkers for Significant Hepatic Fibrosis, Discovery medicine.. 31 (2021) 147-159.

[40] S. Tian, X. Zhou, M. Zhang, et al., Mesenchymal stem cell-derived exosomes protect against liver fibrosis via delivering miR-148a to target KLF6/STAT3 pathway in macrophages, Stem Cell Res. Ther. 13 (2022) 330. https://doi.org/10.1186/s13287-022-03010-y.

[41] X. Luo, Z.X. Xu, J.C. Wu, et al., Hepatocyte-derived exosomal miR-27a activateshepatic stellate cells through the inhibitionof PINK1-mediated mitophagy in MAFLD, Molecular therapy. Nucleic acids. 26 (2021) 1241-1254. https://doi.org/10.1016/j.omtn.2021.10.022.